The study of composition non-uniformity in ternary $Mg_xZn_{1-x}O$ thin films

2003 J. Phys.: Condens. Matter 15 L475

(http://iopscience.iop.org/0953-8984/15/30/102)

INSTITUTE OF PHYSICS PUBLISHING JOURNAL OF PHYSICS: CONDENSED MATTER

J. Phys.: Condens. Matter **15** (2003) L475–L482 PII: S0953-8984(03)62486-0

LETTER TO THE EDITOR

The study of composition non-uniformity in ternary $Mg_xZn_{1-x}O$ thin films

J Chen[1], W Z Shen[1,4], N B Chen[2], D J Qiu[2] and H Z Wu[3]

[1] Laboratory of Condensed Matter Spectroscopy and Opto-Electronic Physics, Department of Physics, Shanghai Jiao Tong University, 1954 Hua Shan Road, Shanghai 200030, People's Republic of China
[2] Department of Physics, Zhejiang University, Hangzhou 310028, People's Republic of China
[3] State Key Laboratory of Functional Materials for Informatics, Shanghai Institute of Microsystem and Information Technology, Chinese Academy of Sciences, Shanghai 200050, People's Republic of China

E-mail: wzshen@sjtu.edu.cn

Received 10 June 2003
Published 18 July 2003
Online at stacks.iop.org/JPhysCM/15/L475

Abstract

We report on the growth of single cubic-phase MgZnO thin films by reactive electron beam evaporation on sapphire substrates. A detailed theoretical procedure has been employed to analyse the transmission profile for information on composition non-uniformity, in addition to the exact determination of the band gap energy. The study of composition non-uniformity has been further extended to both the typically reported hexagonal and cubic MgZnO thin films. It is found that the composition non-uniformity strongly depends on the Mg content, which can be well explained by the ZnO–MgO phase diagram.

Recently, a great deal of research effort on wide band gap semiconductors has resulted in the commercialization of group III nitride-based blue lasers, light emitting diodes and ultraviolet photodetectors [1]. As an alternative to the group III nitride material system, the wide band gap wurtzite ZnO ($E_g \sim 3.37$ eV) [2] and cubic MgO ($E_g \sim 7.50$ eV) [3] and their ternary alloy $Mg_xZn_{1-x}O$ are of substantial interest. The success in both controlled n-type [4] and p-type [5] doping of ZnO and the wide band gap engineering of MgZnO to extremely short wavelengths paves the way for heterostructure device applications, which may eventually compete with the group III nitrides.

According to the phase diagram of the ZnO–MgO binary system [6], the thermodynamic solubility limit of MgO in ZnO has been reported to be less than 4 at.%. However, Ohtomo *et al* [7] demonstrated the first synthesis of high-quality, single-phase $Mg_xZn_{1-x}O$ thin films with Mg concentrations up to 33 at.% due to the non-equilibrium nature of the pulsed laser deposition (PLD) growth. Although there are reports of molecular beam epitaxy (MBE) [8] and

[4] Author to whom any correspondence should be addressed.

metalorganic vapour-phase epitaxy (MOVPE) [9] growth with Mg containing up to 49 at.%, most of the MgZnO thin film growth has been carried out by PLD [7, 10, 11]. It should be noted that all the above-mentioned MgZnO thin films possess hexagonal structure. On the other hand, the phase diagram predicts a solid solution of ZnO in the cubic MgO lattice up to 40 at.%, and very recently, Choopun *et al* [12] and Narayan *et al* [13] reported on the growth of cubic $Mg_xZn_{1-x}O$ thin films grown by PLD, with Mg composition x in the range of 0.50–0.86 and 0.82–1.00, respectively.

The optical properties of MgZnO that have been studied up to now are mainly concerned with transmission/absorption spectra for linear interpolation of the band gap energy [7, 10–13] and photoluminescence measurements for exciton behaviour and alloy broadening [7, 9–11]. For ternary semiconductor materials, the composition non-uniformity has a great influence on device performance. A profound understanding of the composition non-uniformity is also important for the improvement of material quality. Therefore, much attention has been paid to the composition distribution in some important ternary semiconductor materials, such as HgCdTe thin films for mid-infrared detector arrays [14, 15], which is beneficial for a detailed analysis of the transmission profile of the thin films. In MgZnO thin films, the alloying broadening and Stokes' shift have actually been observed due to the composition fluctuation [7, 9]. However, little information is available in the literature on the composition non-uniformity in MgZnO.

In this letter, we report on the growth of cubic $Mg_xZn_{1-x}O$ ($x \sim 0.47$–0.60) thin films by a simple and low-cost method of reactive electron beam evaporation (REBE) and analyse the detailed transmission profile for information on the composition non-uniformity, together with an exact determination of the band gap energy. The study has further been extended to both the typically reported hexagonal and cubic MgZnO thin films. The observed Mg-content-dependent composition non-uniformity can be well understood by the ZnO–MgO phase diagram.

Our $Mg_xZn_{1-x}O$ thin films with different Mg compositions were grown in an REBE system on finely polished sapphire (0001) substrates at low temperature. The sapphire substrates were treated by rinsing in deionized water, boiling in H_2SO_4:H_3PO_4(3:1) for 1 h, rinsing again in deionized water and finally drying by nitrogen. The $(MgO)_x(ZnO)_{1-x}$ target was sintered at 1500 °C by blending the polycrystalline MgO and ZnO powder (each with a purity of 99.9%) into a certain ratio for the evaporation source. Before evaporation the background pressure in the reaction chamber was 5.0×10^{-3} Pa. During MgZnO deposition oxygen gas was introduced into the reaction chamber and the chamber pressure was kept at 5.0×10^{-2} Pa. The substrate temperature was 250 °C and the growth rate was $\sim$8.0 μm h^{-1}, which was calibrated by *ex situ* film thickness measurements using a TENCOR α-step profiler. The ratio of Mg:Zn (at.%) in the MgZnO films was surveyed by using x-ray photoelectron spectroscopy. The thickness of the films studied is about 2 μm. Figure 1 shows the x-ray diffraction (XRD) results (on a Shimadzu XD-3A system with a Cu Kα line) of one $Mg_{0.51}Zn_{0.49}O$ sample. In addition to the diffraction peak at 41.50° due to the (0006) orientation reflection of the sapphire substrate, the peaks at 36.66° with a full width at half maximum (FWHM) of 0.45° and 77.92° with an FWHM of about 1.9° correspond to the (111) and (222) orientation of the cubic $Mg_{0.51}Zn_{0.49}O$, respectively. No signatures of the wurtzite phase (peak at 34.40° for (0002) orientation) were observed in our XRD experiments. These demonstrate that our MgZnO samples all possess single cubic-phase structure. The inset lists all our XRD peak results (full circles), together with the reported cubic MgZnO results in [12] (open diamonds) and [13] (open triangles). It is clear that all the results are close to the cubic MgO diffraction peaks (36.75° and 78.00°, dotted lines). This observation is in agreement with the phase diagram [6], where the lattice constant of NaCl-type MgO–ZnO alloys remains close to that of pure MgO (4.213 Å).

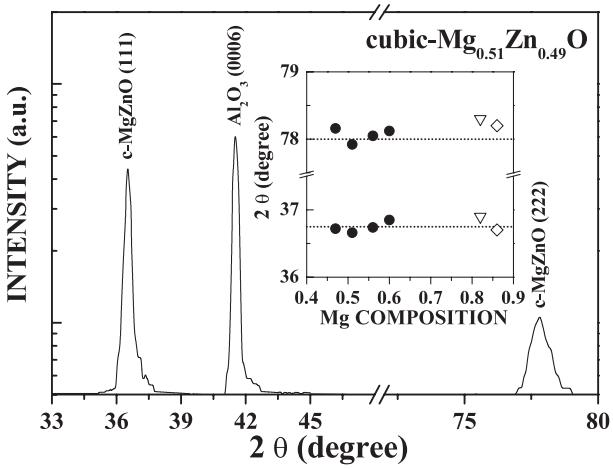

Figure 1. XRD pattern of the cubic $Mg_{0.51}Zn_{0.49}O$ thin film grown by REBE on a sapphire substrate. Shown in the inset are the XRD peak positions of our cubic $Mg_xZn_{1-x}O$ samples (full circles), together with the reported results for the cubic $Mg_{0.86}Zn_{0.14}O$ in [12] (open diamonds) and $Mg_{0.82}Zn_{0.18}O$ in [13] (open triangles). The dotted lines give the pure cubic MgO diffraction peaks of 36.75° and 78.00°.

Figure 2 shows the experimental and theoretical transmission spectra of the cubic $Mg_{0.47}Zn_{0.53}O$ thin film at different temperatures (8 and 300 K). The temperature-dependent transmission measurements of our $Mg_xZn_{1-x}O$ samples were performed on a Jobin-Yvon 460 monochromator with a resolution of 5 Å. In the calculation of the transmission spectra, we consider the multiple reflections between three interfaces: air to $Mg_xZn_{1-x}O$ epilayer (subscript 1), epilayer to transparent sapphire substrate (subscript 2) and substrate to air (subscript 3). The transmission for light passing through the $Mg_xZn_{1-x}O$ thin films can be calculated from

$$T_{1,3} = \frac{(1-R_1)(1-L)T_{2,3}a_1}{1-R_1(1-L)R_{2,3}a_1^2}, \tag{1}$$

where

$$T_{2,3} = \frac{(1-R_2)(1-R_3)a_2}{1-R_2R_3a_2^2}, \tag{2}$$

$$R_{2,3} = R_2 + \frac{R_3(1-R_2)^2a_2^2}{1-R_2R_3a_2^2}, \tag{3}$$

$$a_1 = \exp(-\alpha_{\mathrm{MgZnO}}\, d_{\mathrm{MgZnO}}), \tag{4}$$

$$a_2 = \exp(-\alpha_{\mathrm{sapphire}}\, d_{\mathrm{sapphire}}). \tag{5}$$

The parameter L represents the fraction of light loss at the epilayer surface and is treated as a fixed parameter for every sample to match the maximum measured transmission to the calculated transmission. R_1, R_2 and R_3 are the reflectivities at the three interfaces, respectively, and can be obtained from

$$R = \frac{(n_i - n_j)^2}{(n_i + n_j)^2}. \tag{6}$$

The refractive index n can be obtained from the theoretical calculation for both the MgZnO thin films and the sapphire substrates. Based on a Kramers–Kronig transformation (KKT)

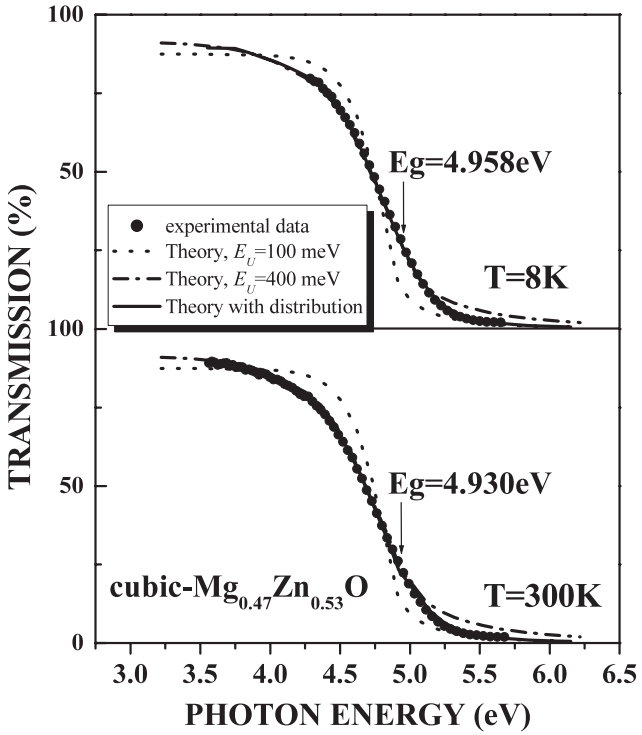

Figure 2. Experimental (full circles) and theoretical (curves) transmission spectra of the cubic $Mg_{0.47}Zn_{0.53}O$ at room temperature (300 K) and low temperature (8 K). The dashed and dash–dotted curves are the calculated results using $E_U = 100$ and 400 meV excluding the composition distribution, respectively. The solid curves are calculated by taking into account the composition distribution and with $E_U = 150$ meV.

model, the real part ε_1 of the complex dielectric function $\varepsilon(E)$ as a function of energy E is described by the sum of four terms. These are the lowest direct gap (E_0) dependence of the interband transition contribution ε_{1i}, the excitonic contribution ε_{1e} at the E_0 critical points, the free-carrier contribution ε_{1f} and the additive constant term $\varepsilon_{1\infty}$, which is a background dielectric contribution arising from the higher-lying gap transitions, such as the E_1, $E_1 + \Delta_1$, and E_2 transitions. The detailed formulae are similar to the ones in our treatment of InN thin films [16]. The complete intrinsic absorption of $Mg_xZn_{1-x}O$ thin films includes both the Urbach exponential absorption edge and intrinsic square-root absorption, and can be written as [17]

$$\alpha(E) = \begin{cases} \alpha_0 \exp[(E - E_e)/E_U] & (E < E_g) \\ \alpha_d (E - E'_g)^{1/2} & (E \geqslant E_g) \end{cases} \tag{7}$$

where E_e coincides roughly with the energy of the lowest free exciton energy at 0 K, E'_g is the band gap energy of the material without band tailing distortions, and E_U is the Urbach band tail parameter. These material parameters, including α_0 and α_d, are linked through the continuity at the band gap energy of E_g.

As shown in figure 2, the above model (excluding the composition distribution) was first employed to fit our transmission spectra. It was found that the band tail parameter E_U is very sensitive to the line shape of the spectra. When $E_U = 100$ meV, the theoretical results (dashed curves) are much steeper than the experimental data and the steepness of the curve decreases

as E_U is increased. Up to $E_U = 400$ meV, the theoretical results (dash–dotted curves) fit the experimental spectra well below the band gap energy. However, the theoretical results do not fit the spectra well in the above band gap energy region, and the overall theoretical curves derived from equations (1)–(7) do not match the experimental data very well, irrespective of how the parameters are adjusted in these equations. This is due to the composition non-uniformity of the $Mg_xZn_{1-x}O$ samples, which is not included in the above model. To make the theory agree better with the experiments, a composition distribution of the epilayer surface should be taken into account. The composition distribution is assumed to obey the normal distribution

$$f(x, x_0) = \frac{1}{\sqrt{2\pi}\sigma} \exp\left(-\frac{[x - x_0]^2}{2\sigma^2}\right), \tag{8}$$

where $f(x, x_0)$ is the probability of Mg composition with value x, x_0 is the average composition, and σ represents the composition deviation. The full curves in figure 2 are calculated by combining the composition distribution (equation (8)) with the theoretical approach (equations (1)–(7)). It is clear that good agreement can be observed throughout the measured photon energy with the adjustable parameters $E_g = 4.930$ eV, $E_U = 150$ meV and $\sigma = 0.05$ at room temperature. Further support of the above consideration is demonstrated in the low temperature transmission spectra. Since the composition deviation σ does not change in the sample, we observe that the theoretical curve matches the experimental data very well at 8 K with $E_g = 4.958$ eV and $E_U = 147$ meV. The band gap energy at 8 K is found to be 0.028 eV larger than that at room temperature, while the weak temperature dependence of the Urbach energy for MgZnO (∼3 meV), as already observed [11], suggests that the main scattering mechanism of optical absorption is due to alloy composition fluctuations. All the temperature-dependent transmission spectra of our samples can be well fitted by employing equations (1)–(8), which clearly demonstrate that the introduction of the composition distribution in MgZnO is reasonable and reliable.

We now extend the above theoretical analysis to the typically reported transmission spectra in both hexagonal [7] and cubic [12, 13] MgZnO thin films for the values of the composition deviation, Urbach band tail, as well as band gap energy. Typical room temperature experimental data (full circles) and our theoretical results (solid curves) are plotted in figure 3. Curve (a) is from our ZnO sample grown by REBE, and the band gap energy obtained is about 3.33 eV, between the reported values of 3.30 eV [7] and 3.37 eV [2]. Curves (b) and (c) are from the PLD-grown hexagonal- and mixed-phase $Mg_xZn_{1-x}O$ with Mg composition equal to 0.25 and 0.36, respectively [7]. Curves (d), (e) and (f) are from our cubic $Mg_xZn_{1-x}O$ with $x = 0.47$, 0.51 and 0.56, respectively. Curves (g) and (h) are from the cubic $Mg_{0.66}Zn_{0.34}O$ and $Mg_{0.71}Zn_{0.29}O$ reported in [12]. The composition distribution has been taken into account in all these theoretical curves except for the binary ZnO sample.

Figure 4(a) illustrates the dependence of the Mg content on the composition deviation σ, which can reveal the composition non-uniformity in MgZnO samples. In hexagonal $Mg_xZn_{1-x}O$ thin films, as x varies from 0 to 0.33 [7], we find that the composition deviation is very small and we can even obtain good fitting results just by using equations (1)–(7). This demonstrates good composition uniformity in hexagonal MgZnO thin films. However, as the Mg content increases, the MgZnO will lie in mixed-phase or cubic-phase regions, where the composition distribution effect has been clearly observed with composition deviation σ in the range from 0.046 to 0.088 in cubic $Mg_xZn_{1-x}O$ ($x \sim 0.45$–0.66) thin films. Furthermore, it is interesting to note that the composition deviation decreases with increasing Mg content in these cubic-phase structures, e.g. for $Mg_{0.71}Zn_{0.29}O$ [12] and $Mg_{0.82}Zn_{0.18}O$ [13], the value of σ decreases to 0.036 and 0.020, respectively. According to the phase diagram of the ZnO–MgO binary system [6], although there are certain percentages of thermodynamic solid solubility of

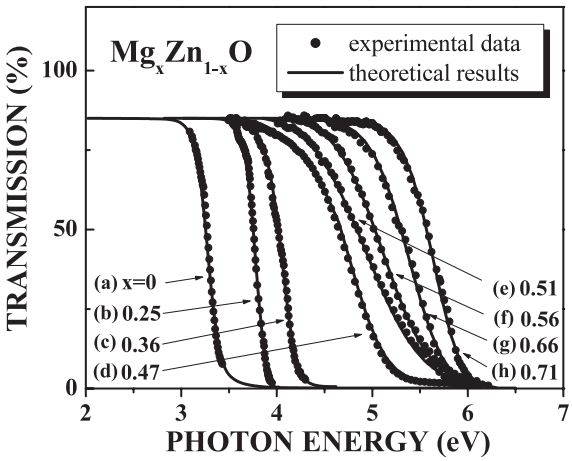

Figure 3. Experimental (full circles) and theoretical (solid curves) transmission spectra of both hexagonal ($0 \leqslant x \leqslant 0.33$) and cubic ($0.45 \leqslant x \leqslant 1.0$) $Mg_xZn_{1-x}O$ thin films at room temperature.

MgO in ZnO and ZnO in MgO, the large structural dissimilarity between the wurtzite hexagonal ZnO and NaCl-type cubic MgO results in an unstable condition in MgZnO with intermediate Mg content. A phase separation into MgO and ZnO takes place in hexagonal MgZnO thin films [7, 10, 12, 13]. Observation of composition distribution behaviour in the intermediate Mg content range clearly reveals the phase diagram results. An increase of composition deviation σ with Mg composition reflects the structural phase transition from wurtzite via the mixed-phase region to the cubic one. In contrast, as the Mg content is close to the cubic binary MgO, the cubic-phase MgZnO will become more and more stable, displaying a clear decrease in composition deviation σ.

The band tail parameter E_U is found to increase with Mg composition x, which indicates more randomness in the alloys with higher Mg content. The obtained values of band tail parameter $E_U = 36$ meV ($x = 0.03$), 40 meV ($x = 0.07$), 49 meV ($x = 0.14$), 60 meV ($x = 0.25$), 100 meV ($x = 0.36$) and ~150 meV for cubic structures are in good agreement with the reported results [11]. The yielded band gap energies are shown in figure 4(b) as a function of Mg composition (full circles) for both the hexagonal- and cubic-phase $Mg_xZn_{1-x}O$ thin films. We can use the two different linear functions (solid lines) to summarize the band gap relationship in $Mg_xZn_{1-x}O$ alloys for x varying from 0 to 0.82:

$$E_g(Mg_xZn_{1-x}O) = 3.32 + 2.00x \qquad \text{(for hexagonal-phase, } 0 \leqslant x \leqslant 0.33\text{)}, \tag{9}$$

$$E_g(Mg_xZn_{1-x}O) = 3.02 + 4.03x \qquad \text{(for cubic-phase, } 0.45 \leqslant x \leqslant 0.82\text{)}. \tag{10}$$

It is interesting to note that the slope of the cubic MgZnO line is double that of the hexagonal MgZnO, which is the manifestation of favourable band gap engineering in cubic MgZnO thin films. We think that the E_g values obtained through our detailed calculations above are more reliable than that from the normally linear extrapolated method. The open circles and the dotted lines in figure 4(b) are the band gap energies and their linear fits obtained from the simply linear extrapolation [7, 12]. They are about 0.07 and 0.14 eV higher than the values from our detailed transmission profile calculation, respectively, although the two sets of lines, as expected, each have almost the same slope. Finally, we mention the quality of our REBE-grown MgZnO samples. It is clear that the observed optical properties, such as the band gaps, the Urbach band tails and the XRD results, are in good agreement with the single crystal data given in the literature [7, 10–13]. Furthermore, we note that the composition deviation in

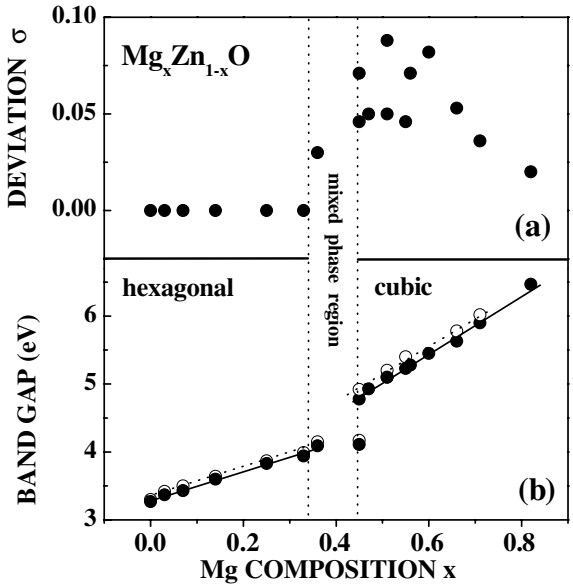

Figure 4. Summary of the dependence of Mg content on (a) the composition deviation σ and (b) the band gap energies in MgZnO thin films. The band gap energies from the linear interpolation method in [7] and [12] are also shown (as open circles) for comparison.

our cubic MgZnO thin films is similar to the value in the cubic MgZnO thin films grown by PLD [12] with the same level of Mg composition ($x \sim 0.45$–0.66). These conclusions give us confidence that our REBE-grown MgZnO thin films are also of good quality, which clearly demonstrates the suitability of growing MgZnO thin films by the simple and low-cost REBE method.

In summary, good-quality single cubic-phase MgZnO thin films have been grown by the simple and low-cost REBE method on sapphire substrates. A detailed theoretical procedure has been employed to analyse the transmission profile for information on composition non-uniformity in both the typically reported hexagonal and cubic MgZnO thin films, in addition to the exact determination of the band gap energy. We find that the composition non-uniformity in hexagonal MgZnO is very small and the composition deviation decreases with increasing Mg content in cubic MgZnO, in agreement with predictions of the ZnO–MgO phase diagram. We also give the more reliable Mg composition-dependent band gap energies for both the hexagonal- and cubic-phase $Mg_xZn_{1-x}O$ thin films.

This work was supported in part by the Natural Science Foundation of China under the contracts of 10125416 and 10174064, and HYD (No 81005), TRAPOYT of the National Minister of Education.

References

[1] Nakamura S and Fasol G 1997 *The Blue Laser Diode* (Berlin: Springer)
[2] Kaldis E (ed) 1981 *Current Topics in Materials Science* vol 7 (Amsterdam: North-Holland) pp 143–482
[3] Roessler D M and Walker W C 1966 *Phys. Rev. Lett.* **17** 310
[4] Makino T, Tamure K, Chia C H, Segawa Y, Kawasaki M, Ohtomo A and Koinuma H 2002 *Phys. Status Solidi* b **229** 853

[5] Choopun S, Vispute R D, Noch W, Balsamo A, Sharma R P, Venkatesan T, Iliadis A and Look D C 1999 *Appl. Phys. Lett.* **75** 3947
[6] Segnit E R and Holland A E 1965 *J. Am. Ceram. Soc.* **48** 412
[7] Ohtomo A, Kawasaki M, Koida T, Masubuchi K, Koinuma H, Sakurai Y, Yoshida Y, Yasuda T and Segawa Y 1998 *Appl. Phys. Lett.* **72** 2466
[8] Ohtomo A, Kawasaki M, Sakurai Y, Ohkubo I, Shiroki R, Yoshida Y, Yasuda T, Segawa Y and Koinuma H 1998 *Mater. Sci. Eng.* B **56** 263
[9] Park W I, Yi Gyu-Chul and Jang H M 2001 *Appl. Phys. Lett.* **79** 2022
[10] Sharma A K, Narayan J, Muth J F, Teng C W, Jin C, Kvit A, Kolbas R M and Holland O W 1999 *Appl. Phys. Lett.* **75** 3327
[11] Teng C W, Muth J F, Ozgur U, Bergmann M J, Everitt H O, Sharma A K, Jin C and Narayan J 2000 *Appl. Phys. Lett.* **76** 979
[12] Choopun S, Vispute R D, Yang W, Sharma R P and Venkatesan T 2002 *Appl. Phys. Lett.* **80** 1529
[13] Narayan J, Sharma A K, Kvit A, Jin C, Muth J F and Holland O W 2002 *Solid State Commun.* **121** 9
[14] Chu J H, Miao J W, Shi Q, Liu K and Ji H M 1992 *Chin. J. Infrared Millimetre Waves* **11** 411
[15] Hougen C A 1989 *J. Appl. Phys.* **66** 3763
[16] Jiang L F, Shen W Z, Yang H F, Ogawa H and Guo Q X 2003 *Appl. Phys.* A **77** at press (Online 22 January 2003 at http://www.link.springer-ny.com/link/service/journals/00339/first/bibs/s00339-002-2002-7.htm)
[17] Shen W Z 2002 *Int. J. Infrared Millimetre Waves* **23** 61